Role for hepatic CEACAM1 in regulating fatty acid metabolism along the adipocyte-hepatocyte axis[S]

Lucia Russo,[1,*] Hilda E. Ghadieh,[1,*] Simona S. Ghanem,[1,*] Qusai Y. Al-Share,[*] Zachary N. Smiley,[*] Cara Gatto-Weis,[*,†] Emily L. Esakov,[*,§] Marcia F. McInerney,[*,§] Garrett Heinrich,[*,] Xin Tong,[††] Lei Yin,[††] and Sonia M. Najjar[2,*,**]**

Center for Diabetes and Endocrine Research,[*] and Department of Pathology,[†] College of Medicine and Life Sciences, and Department of Medicinal and Biological Chemistry at the College of Pharmacy and Pharmaceutical Sciences,[§] University of Toledo, Toledo, OH 43614; Department of Molecular and Integrative Physiology,[††] University of Michigan Medical School, Ann Arbor, MI 48019; and Department of Biomedical Sciences, Heritage College of Osteopathic Medicine,[**] Ohio University, Athens, OH 45701

Abstract **Carcinoembryonic antigen-related cell adhesion molecule 1 (CEACAM1) regulates insulin sensitivity by promoting hepatic insulin clearance and mediating suppression of fatty acid synthase activity. Feeding C57BL/6J male mice with a high-fat (HF) diet for 3–4 weeks triggered a >60% decrease in hepatic CEACAM1 levels to subsequently impair insulin clearance and cause systemic insulin resistance and hepatic steatosis. This study aimed at investigating whether lipolysis drives reduction in hepatic CEACAM1 and whether this constitutes a key mechanism leading to diet-induced metabolic abnormalities. Blocking lipolysis with a daily intraperitoneal injection of nicotinic acid in the last two days of a 30-day HF feeding regimen demonstrated that white adipose tissue (WAT)-derived fatty acids repressed hepatic CEACAM1-dependent regulation of insulin and lipid metabolism in 3-month-old male C57BL/6J mice. Adenoviral-mediated CEACAM1 redelivery countered the adverse metabolic effect of the HF diet on insulin resistance, hepatic steatosis, visceral obesity, and energy expenditure. It also reversed the effect of HF diet on inflammation and fibrosis in WAT and liver. This assigns a causative role for lipolysis-driven decrease in hepatic CEACAM1 level and its regulation of insulin and lipid metabolism in sustaining systemic insulin resistance, hepatic steatosis, and other abnormalities associated with excessive energy supply.**—Russo, L., H. E. Ghadieh, S. S. Ghanem, Q. Y. Al-Share, Z. N. Smiley, C. Gatto-Weis, E. L. Esakov, M. F. McInerney, G. Heinrich, X. Tong, L. Yin, and S. M. Najjar. **Role for hepatic CEACAM1 in regulating fatty acid metabolism along the adipocyte-hepatocyte axis.** ***J. Lipid Res.*** **2016.** 57: **2163–2175.**

Supplementary key words carcinoembryonic antigen-related cell adhesion molecule 1 • insulin resistance • nicotinic acid • lipolysis • insulin clearance

Circulating insulin levels, in part determined by hepatic insulin clearance, regulate insulin action (1–3). Insulin clearance, which occurs mostly in liver and to a lower extent in kidney, but not in skeletal muscle or white adipose tissue (WAT), plays a pivotal role in promoting insulin sensitivity (4). If impaired, it contributes to mounting hyperinsulinemia in obese humans (5, 6), thus constituting a risk factor for metabolic syndrome (7, 8).

Our studies on the carcinoembryonic antigen-related cell adhesion molecule 1 (CEACAM1), a transmembrane glycoprotein that is highly expressed in liver and kidney, but not WAT or skeletal muscle (9), support these findings. Upon its phosphorylation by the insulin receptor, CEACAM1 promotes insulin clearance by upregulating receptor-mediated insulin uptake into clathrin-coated pits and degradation in hepatocytes (10). Moreover, it mediates a downregulatory effect on mouse fatty acid synthase

This work was supported by the following grants from the National Institutes of Health: National Institute of Diabetes and Digestive and Kidney Diseases Grants R01 DK054254 (S.M.N.), R01 DK083850 (S.M.N.), K99/R00-DK077449 (L.Y.), R01 DK099593 (L.Y.), and R15 DK103196 (M.F.M.); and National Heart, Lung, and Blood Institute Grant R01 HL112248 (S.M.N.). The content is solely the responsibility of the authors and does not necessarily represent the official views of the National Institutes of Health. The work was also supported by fellowships from the American Heart Association (14POST20480294 [L.R.]) and the Middle-East Diabetes Research Center (H.E.G. and S.S.G.). No conflict of interest relevant to this work was reported.

Manuscript received 16 September 2016 and in revised form 17 October 2016.

Published, JLR Papers in Press, October 24, 2016
DOI 10.1194/jlr.M072066

Abbreviations: Ad-GFP, adenovirus construct bearing green fluorescent protein control cDNA; Ad-rSA, adenovirus construct bearing the S503A phosphorylation-defective CEACAM1 mutant cDNA; Ad-rWT, adenovirus construct bearing wild-type rat CEACAM1 cDNA; AUC, area under the curve; BAT, brown adipose tissue; BW, body weight; CEACAM1, carcinoembryonic antigen-related cell adhesion molecule 1; Ceacam1, mRNA transcripts of CEACAM1; *Ceacam1*, mouse gene encoding CEACAM1 protein; *Cc1*$^{-/-}$, mice with null deletion of *Ceacam1*; DAPI, 4',6-diamidino-2-phenylindole; Fasn, mouse fatty acid synthase; FATP, fatty acid transport protein; H and E, hematoxylin and eosin; HF, high fat; IL, interleukin; NA, nicotinic acid; qRT-PCR, quantitative RT-PCR; RD, regular standard diet; RER, respiratory exchange rate; TGF-β, transforming growth factor-β; WAT, white adipose tissue.

[1] L. Russo, H. E. Ghadieh, and S. S. Ghanem contributed equally to this article.

[2] To whom correspondence should be addressed.
e-mail: najjar@ohio.edu

[S] The online version of this article (available at http://www.jlr.org) contains a supplement.

(Fasn) activity in response to acute rise in insulin in the first hour of refeeding following an overnight fast (11). This positions CEACAM1 to contribute to the regulation of fatty acid oxidation until glycogen repletion is complete (12). Mice with null deletion of *Ceacam1* (*Cc1*$^{-/-}$) or with liver-specific inactivation of CEACAM1 develop hyperinsulinemia, caused by impaired insulin clearance, followed by insulin resistance, hepatic steatosis, and visceral obesity (13–16). Normal acute-phase insulin release to glucose and intact β-cell function support the observation that chronic hyperinsulinemia is mainly driven by impaired insulin clearance in *Cc1*$^{-/-}$ mutants (15).

Studies in mice (17), dogs (18), and humans (19) demonstrated that defective hepatic insulin clearance is involved in diet-induced insulin resistance. Providing a Western-style diet caused rapid hepatic insulin resistance in healthy young South Asian men but not Caucasians, in association with altered insulin clearance in the Asian group (19). We have shown that high fat (HF) reduced hepatic CEACAM1 level by >60% and impaired insulin clearance in WT mice within 3 weeks to introduce metabolic abnormalities that were prevented by forced transgenic fat-inducible CEACAM1 overexpression in liver (17). The clinical implication of our studies is underscored by the observed low hepatic CEACAM1 level in obese, insulin-resistant subjects with fatty liver disease (20).

Dietary fatty acids can reach the liver via chylomicrons in addition to lipolysis in WAT. In uncomplicated human obesity with low-grade insulin resistance, lipolysis-derived fatty acids are mainly removed by oxidation in the liver (21). Lipolysis occurs within few days of the initiation of HF intake, owing to dysregulated hypothalamic control, even in the absence of insulin resistance in WAT (22). This could cause rapid hepatic insulin resistance (portal hypothesis) via several mechanisms (23), including protein kinase Cδ-mediated pathways (24). With persistent nutritional burden, hepatic lipotoxicity and systemic insulin resistance develop in parallel to the progression of a proinflammatory state in WAT (25).

Release of fatty acids during an acute intralipid infusion reduced hepatic CEACAM1 levels and impaired insulin clearance (24). Thus, we herein investigated the role of lipolysis-derived fatty acids in the suppression of CEACAM1 by HF diet and assessed the significance of this mechanism in diet-induced metabolic abnormalities.

MATERIALS AND METHODS

Mice maintenance

C57BL/6J mice were kept in a 12 h dark/light cycle. As reported (17), male mice (3 months old) were housed as 3–4 mice/cage and fed ad libitum for 30 days a standard chow [regular standard diet (RD)] or an HF diet deriving 45:35:20% calories from fat-carbohydrate-protein (catalog #D12451, Research Diets). On day 28, some HF-fed mice were subjected to a once daily intraperitoneal injection of nicotinic acid (NA) [200 mg/kg body weight (BW)/day] (Sigma-Aldrich) for 2 days (26, 27). The Institutional Animal Care and Utilization Committee approved all procedures.

Metabolic parameters

Mice were overnight fasted, and their retroorbital venous blood was drawn at 1100 h the following morning to assess blood, plasma, and tissue biochemistry, as previously described (17).

Insulin and glucose tolerance tests

Mice were fasted for 6 h before being injected intraperitoneally with Human Regular Insulin (0.75 U/kg BW, Novo Nordisk) (for insulin tolerance) or glucose (1.5 g/kg BW of 50% dextrose solution, Dextrose Injection, USP). Glucose was measured in tail blood at 0–180 min postinjection.

Indirect calorimetry analysis

Mice were individually caged for 5 days (CLAMS system, Columbus Instrument), and their spontaneous physical activity was determined on the X-(locomotor), Y-(ambulatory), and Z-(standing) axes (17). Oxygen consumption (VO_2), CO_2 production (VCO_2), and heat production were sampled every 20 min and normalized to lean mass. The respiratory exchange rate (RER) was calculated as the VCO_2/VO_2 ratio. Heat production was calculated as $Cv \times VO_2$ normalized to lean body mass; with Cv (calorific value) being: $3.815 + 1.232 \times RER$. Data were represented as mean ± SEM of light (700 h-1900 h) and dark (1900 h-700 h) cycles.

Fatty acid synthase activity

As previously described (11), livers were homogenized in buffer containing 20 mM Tris (pH 7.5), 1.0 mM EDTA, 1.0 mM DTT, and phosphatase and protease inhibitors (11). Following centrifugation at 12,500 *g* for 30 min, 10 μl of the supernatant was added to 65 μl of the reaction mix. This contains: 166.6 μM acetyl-CoA, 100 mM potassium phosphate (pH 6.6), 0.1 μCi [^{14}C] malonyl-CoA (Perkin Elmer, Waltham, MA), and 25 nmol malonyl-CoA, in the absence (negative controls) or presence of 500 μM NADPH (Sigma Aldrich). A 1:1 chloroform-methanol solution was used to stop the reaction. Following centrifugation, the supernatant was vacuum-dried, and the pellet resuspended in 200 μl of water-saturated butanol. To reextract the upper layer, 200 μl of ddH_2O was added followed by vortexing and spinning for 1 min. The butanol layer was extracted, dried, and counted for the incorporation of radiolabeled malonyl-CoA into palmitate. Fasn activity was calculated as cpm of [^{14}C] incorporated per microgram of cell lysates, and the protein concentration was determined by Bio-Rad protein assay.

Ex vivo palmitate oxidation

As previously described (28) with some modifications, mice were fasted overnight and anesthetized, and the liver removed, weighed, and homogenized in 10 mM Tris (pH 7.2), 300 mM sucrose, and 2 mM EDTA. Then 1 ml of the homogenate was added to a sealed beaker containing 1 ml of solution A and left at 30°C for 45 min. Solution A: 0.2 mM of [1-^{14}C]palmitate (0.5 mCi/ml) (American Radiolabeled Chemicals Inc.) and 2 mM ATP in incubation buffer (100 mM sucrose, 10 mM Tris-HCl, 5 mM potassium phosphate, 80 mM KCl, 1 mM $MgCl_2$, 2 mM L-carnitine, 0.1 mM malic acid, 0.05 mM CoA, 1mM dithiothreitol, 0.2 mM EDTA, and 0.5% BSA, pH 7.4). Benzothonium hydroxide (Sigma-Aldrich) was added to a basket attached to the sealed beaker and the reaction was terminated with perchloric acid to recover the radioactive acid soluble metabolites (29). Trapped CO_2 radioactivity and the partial oxidation products were measured by liquid scintillation in CytoCint (MP Biomedicals). The oxidation rate was expressed as the sum of total and partial fatty acid oxidation expressed in nanomoles per gram per minute.

Gomori-trichrome staining

Trichrome stain was performed on formalin-fixed adipose tissue using the Thermo Scientific Richard-Allan Scientific Chromaview-advanced Testing (30). Adipose tissue was fixed in 10% formalin and replaced by 70% ethanol before undergoing blocking in paraffin. Sections were deparaffinized at 60°C and hydrated in deionized water. Slides were then stained with Bouin's Fluid at 56°C for 45 min, followed by rinsing in deionized water to remove the yellow color. Slides were placed in Working Weigert's Iron Hematoxylin at room temperature for 10 min followed by Trichrome Stain for 15 min, dehydrated sequentially in 1% acetic acid solution for 1 min, 95% ethanol for 30 s, and 100% ethanol for 1 min (twice). Sections were cleared in xylene 3 times for 1 min each and mounted.

Immunofluorescence

Whole WAT was formalin-fixed for 24 h, transferred to Dulbecco's PBS (Sigma-Aldrich) at 4°C, and permeabilized in 1% TritonX-100/PBS for 15 min before staining macrophages with rat anti-mouse F4/80 (Invitrogen) and detecting with donkey anti-rat IgG-conjugated to Alexa-Fluor488. Tissues were incubated with primary antibodies overnight at 4°C then washed 3× with PBS-Tween20 before applying the secondary stain for 2 h at room temperature and washing 3× in PBS-Tween. Stained samples were then counterstained for 25 min at room temperature with 5 μM BODIPY-558/568 (Molecular Probes) and Hoechst stain/4',6-diamidino-2-phenylindole (DAPI) (Invitrogen) to visualize lipid and nuclei, respectively. Samples were placed on a coverslip and imaged using a Leica-TCS-SP5 laser-scanning microscope equipped with conventional solid-state and a Ti-sapphire tunable multiphoton laser (Coherent). Images were acquired in the 3D-XYZ plane in 4 μm steps with a 63× objective (NA-0.70) using the sequential scan mode to eliminate any spectral overlap in individual fluorophores. Specifically, Alexa-Fluor488 was excited at 488 nm with collection at 500–558 nm. The BODIPY-558/568 dye was excited at 561 nm and collected at 567–609 nm. Selected images are a 2D-representation of the 3D-laser scanning confocal microscopy-image stack as labeled.

Western blot analysis

Proteins were analyzed by SDS-PAGE and immunoprobing with polyclonal antibodies against α-Fasn (Cell Signaling Technology), phospho-Akt (Ser^{473}), and phospho-Akt2 (p-Akt2) followed by α-Akt or α-Akt2, respectively; custom-made polyclonal antibodies raised in rabbit against mouse CEACAM1 (α-mCC1 Ab3759) (17), rat CEACAM1 [(αP_3(488)], and phoshpo-CEACAM1 (α-pCC1) (24). For normalization, monoclonal antibodies against actin or GAPDH (Santa Cruz Biotechnology) were used. Blots were incubated with horseradish peroxidase-conjugated goat anti-mouse or anti-rabbit IgG (GE Healthcare Life Sciences, Amersham) antibodies and subjected to ECL (Amersham Pharmacia Biotech) and quantification by densitometry and Image J software (v. 1.40, National Institutes of Health).

For coimmunoprecipitation, liver lysates (35 μg) were immunoprecipitated with α-Fasn antibody, followed by analysis on 5% SDS-PAGE and sequential immunoblotting with α-mCC1 and α-Fasn antibodies.

Primary hepatocytes isolation and fatty acid treatment

Hepatocytes were isolated by perfusing liver (1 ml/min) with Collagenase-Type II (1 mg/ml) (Worthington) (13). Cells were dispensed in Williams-E complete media (Gibco) containing 10 mM lactate, 10 nM dexamethasone, 100 nM insulin (Sigma Aldrich), 10% FBS, and 1% penicillin-streptomycin (Gibco). Cells were plated onto 12-well plates at 2.5×10^5/well and incubated at 37°C in Williams-E medium for 24 h before switching to phenol red-free Williams-E medium-supplemented with 10% dialyzed FBS, 1% penicillin-streptomycin for 24 h. A fatty acid mixture resembling the dietary fat composition (0.1 mM) was added for 24 h: 0.035 mM palmitate, 0.045 mM oleate, 0.02 mM linoleate-2 mM insulin-free BSA (Sigma Aldrich) at a 1:5 ratio], supplemented with 10 mM lactate.

Luciferase assay

As described (12), Hepa1-6 mouse-derived cells were seeded at 4.0×10^5 into 6-well plates and at ~60–70% confluence, a 24 h transfection was performed with 500 ng of promoter constructs containing the WT sequence spanning 1100 nucleotides or the **Δ**PPRE/RXR mutant carrying a mutation between nucleotides –557 and –543 (5′-CAATTCTATGAAATC-3′) and 10 ng of *renilla* luciferase (pRL-TK, Promega) using Fugene 6 (Promega). Empty pGL4.10 vector was used as negative control. Cells were then serum-starved, treated with ethanol (Veh) or 0.1 mM FA (above) for 24 h. Luciferase activity was assessed using the Dual-Luciferase Reporter Assay System (Promega).

Adenovirus preparation and cell transduction

The construction of the adenovirus vectors harboring WT and the phosphorylation-defective serine503-to-alanine (S503A) rat CEACAM1 mutant was described (15). Adenoviruses were produced in 293AD packaging cells (Agilent Technologies) following LipofectAMINE-mediated transfection (Invitrogen) and concentrated by ultracentrifugation in cesium chloride gradient (31). Adenoviral-mediated CEACAM1 overexpression was confirmed by transducing primary mouse hepatocytes prepared from C57BL/6J mice at 1×10^7 particles/well of a 6-well plate for 36 h. CEACAM1 level was determined by immunoblotting with anti-rat CEACAM1 antibody (24).

Tail-vein injection of recombinant adenovirus to redeliver CEACAM1 to the liver

Two-month-old C57BL/6J mice were HF fed for 20 days before being subjected to adenoviral infection by tail-vein injection of 1×10^{10} particles/mouse and housed individually for 21 days. The control group was injected with adenovirus construct bearing green fluorescent protein control cDNA (Ad-GFP) at the same viral titer. Insulin and glucose tolerance were performed 13 and 16 days postinjection, as described below. Mice were subjected to indirect calorimetry before being euthanized at 21 days postinjection.

Real-time quantitative RT-PCR

Total RNA was isolated with PerfectPure RNA Tissue Kit (5 PRIME Inc.) and cDNA was synthesized by iScript cDNA Synthesis Kit (BIO-RAD), using 1 μg of total RNA and oligodT primers (supplemental Table S1). cDNA was evaluated with quantitative RT-PCR (qRT-PCR; StepOne Plus, Applied Biosystems), and mRNA was normalized to 18S or Gapdh, as previously described (17).

Statistical analysis

Data were analyzed by one-way ANOVA with Bonferroni correction, using GraphPad Prism 6 software. $P < 0.05$ was statistically significant.

RESULTS

NA inhibits lipolysis and causes fat accumulation in WAT

To investigate the role of adipocyte-derived fatty acids in diet-induced metabolic abnormalities, mice were HF fed and treated with NA or saline (S) in the last 2 days of feeding. Relative to RD, HF induced BW, visceral and total fat mass, including brown adipose tissue (BAT) mass with a reciprocal decrease in lean mass (**Table 1**, HF-S vs. RD-S).

TABLE 1. Effect of NA on plasma and tissue biochemistry

	RD-S	HF-S	HF-NA
BW (g)	24.7 ± 0.9	29.2 ± 1.0[a]	28.0 ± 0.3[a]
% Fat mass (NMR)	0.8 ± 0.2	6.7 ± 1.3[a]	10.1 ± 0.5[a,b]
% Lean mass (NMR)	71.5 ± 0.4	67.6 ± 1.2[a]	64.6 ± 0.5[a,b]
% Visceral fat (WAT/BW)	0.8 ± 0.2	2.2 ± 0.4[a]	2.7 ± 0.2[a]
% BAT/BW	3.5 ± 0.6	8.5 ± 1.1[a]	11.0 ± 0.9[a]
Hepatic triacylglycerol (μg/mg)	36.3 ± 4.1	56.5 ± 5.8[a]	32.1 ± 3.0[b]
Plasma NEFA (mEq/l)	0.6 ± 0.1	0.9 ± 0.1[a]	0.6 ± 0.0[b]
Plasma triacylglycerol (mg/dl)	109.1 ± 10.2	134.4 ± 12.1	120.3 ± 13.3
Plasma insulin (Ins) (pM)	64.4 ± 5.8	89.0 ± 8.0[a]	62.2 ± 5.0[b]
Plasma C-peptide (pM)	475.4 ± 98.2	514.3 ± 123.1	548.2 ± 114.2
Plasma C-peptide/Ins molar ratio	6.0 ± 0.4	4.1 ± 0.4[a]	6.5 ± 0.4[b]
Fasting blood glucose (mg/dl)	101 ± 4	99 ± 8	99 ± 12
Fed blood glucose (mg/dl)	101 ± 3	127 ± 3[a]	101 ± 3[b]
Fed plasma leptin (ng/ml)	0.7 ± 0.1	3.5 ± 1.1[a]	2.8 ± 0.4[a]

Male mice (n = 6–10/feeding/treatment group) were fed RD or HF diet for 30 days. In the last 2 days of feeding, mice were treated with NA, and their body fat composition evaluated by nuclear magnetic resonance (NMR; Bruker Optics). Except for leptin and fed blood glucose levels, mice were fasted overnight for 18 h and their tissues extracted to assess visceral and brown fat mass relative to BW, and blood was drawn to determine plasma levels of NEFA, triacylglycerol, Ins, and C-peptide levels. Values are expressed as mean ± SEM.

[a] $P < 0.05$ versus RD-S.

[b] $P < 0.05$ HF-NA versus HF-S.

Consistently, HF increased fasting plasma NEFA (Table 1) and the mRNA level of hormone sensitive lipase (Hsl) in WAT (12.7 ± 0.56 in HF-S vs. 6.77 ± 1.07 in RD-S mice; $P < 0.05$). As expected, NA treatment restored plasma NEFA (Table 1) and Hsl mRNA levels (3.75 ± 0.60 in HF-NA vs. 12.7 ± 0.56 in HF-S mice; $P < 0.05$) but maintained the gain in visceral obesity and BW in response to HF (Table 1). Consistently, plasma leptin levels remained elevated in HF-NA relative to RD-S mice (Table 1).

Histological analysis of hematoxylin and eosin (H and E)-stained WAT sections (**Fig. 1A**) confirmed the maintenance of adipocytes' expansion to accommodate fat storage in WAT derived from HF-NA mice (adipocyte size of 2,078 ± 86 μm^2 in HF-NA vs. 1,848 ± 91 in HF-S and 576 ± 23 in RD-S).

NA reverses diet-induced fibrosis in WAT

Because visceral obesity is associated with increased fibrosis in WAT in rodents (32, 33) and humans (34), we then examined whether NA treatment modulates HF-induced fibrosis in WAT. HF induced the mRNA levels of profibrogenic effectors: endotrophin/Col6α3, a protein that promotes metabolic derangement and fibrosis in adipose tissue (33), α-smooth muscle actin (α-Sma), and transforming growth factor-β (Tgf-β) (supplemental Table S2; HF-S vs. RD-S). In contrast, HF lowered the mRNA level of Smad7 that inhibits TGF-β signaling (35, 36) (supplemental Table S2; HF-S vs. RD-S). NA treatment reversed the effect of HF, with a lesser extent in Col6α3 mRNA relative to other markers (supplemental Table S2). This translated into limiting HF-induction of collagen deposition in WAT by NA, as indicated by Trichrome-C staining (Fig. 1B).

NA induces macrophage inflammation in WAT of HF-fed mice

qRT-PCR analysis in WAT revealed induction of mRNA of macrophages (CD68 and F4/80) and TNF-α by HF, but without significantly changing the expression of other proinflammatory markers such as interleukin (IL)-1β, IL-6, and IFN-γ (supplemental Table S2). NA further induced the mRNA levels of these markers by ~2- to 3-fold. Immunofluorescence analysis of F4/80 (green) in WAT showed evidence of macrophage inflammation in HF-S and HF-NA compared with RD-S mice (Fig. 1C-viii and ix vs. vii). In contrast to RD-fed mice (Fig. 1C-x), HF induced macrophage staining around the adipocytes (gray), but to a higher extent in NA-treated versus saline-treated mice (Fig. 1C-xii vs. xi), indicating increased macrophage inflammation by NA. Despite fewer macrophages; however, HF-S mice displayed higher plasma NEFA levels than HF-NA (Table 1).

NA reverses diet-induced insulin resistance

Consistent with our previous report (17), HF caused insulin resistance, as indicated by fed hyperglycemia (Table 1) and intolerance to exogenous insulin in HF-S versus RD-S [**Fig. 2A** and accompanying graph of the area under the curve (AUC)]. Both glucose levels (Table 1) and insulin tolerance (Fig. 2A) were restored by NA treatment. To further examine insulin action, we refed mice for 7 h after an overnight fast to allow insulin release (Fig. 2B-i). Immunoblotting (Ib) with phosphoAkt antibody (symbol-pAkt) revealed blunted insulin's ability to phosphorylate Akt at 7 h of refeeding (RF) relative to overnight-fasted mice (F) in lysates from liver (Fig. 2B-ii), but not WAT (Fig. 2B-iii) of HF-fed mice. NA treatment restored insulin-induced Akt phosphorylation in liver (Fig. 2B-ii) but blunted it in WAT of HF-fed mice (Fig. 2B-iii).

NA restores insulin clearance in HF-fed mice

Western blot analysis of liver lysates revealed reduction of CEACAM1 (CC1) protein level by ~>60% in HF-S versus RD-S mice (Fig. 2C-i). This was restored by NA treatment (Fig. 2C-i, HF-NA vs. RD-S). Subsequently, this normalized insulin clearance, assessed by the higher steady-state C-peptide/insulin molar ratio (Table 1; HF-NA vs. HF-S) and

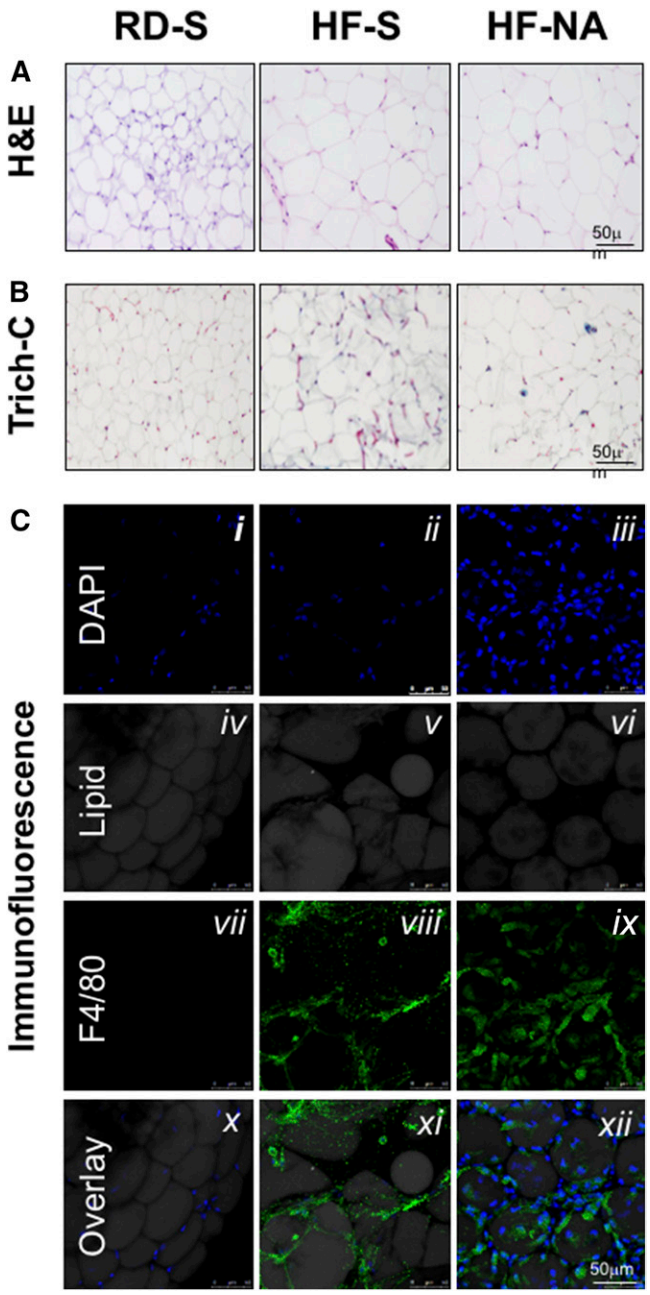

Fig. 1. Effect of NA on fat accumulation, fibrosis and inflammation in WAT. A: H and E staining of the WAT from mice fed ad libitum either with an RD or an HF diet for 30 days. In the last 2 days of feeding, RD-fed mice were administered a once daily intraperitoneal injection of saline (S) while HF-fed mice were treated with either saline or NA (n > 6 mice/feeding/treatment group). B: Trichrome C (Trich-C) stain was used to assess fibrosis in WAT. Black staining indicates nuclei. Cytoplasm and fibers are in red. Collagen is shown in blue. Representative images from three sections/mouse are shown (20× magnification). C: Whole WAT was stained with BODIPY 558/568 to detect lipid (gray) for staining of adipocytes and with anti-F4/80 to detect macrophages (green). Nuclei from cells, including macrophages and adipocytes, were stained with DAPI (blue). All images were captured using laser scanning confocal microscopy with a 63× objective and are 2D projections of a 3D image z-stack. Increased DAPI staining indicating cellular inflammation is observed in HF-NA (*iii*) compared with RD-S (*i*) or HF-S (*ii*) treated animals. F4/80 staining was elevated in HF-NA (*ix*) compared with HF-S (*viii*) indicating increased inflammation in HF-NA treated mice, while there was no F4/80 staining in RD-S. The overlay shows that nuclei and macrophages surrounding adipocytes are increased in the HF-NA treated mice (*xii* vs. *xi*) indicating increased inflammation in the HF-NA treated mice compared with the HF-S treated or RD-S treated mice. Representative images from three sections per mouse per each staining are shown. The scale bar on the last panel of each stain represents scale bar in all other panels per stain.

lowered plasma insulin levels (Table 1), in parallel to restoring insulin sensitivity (Fig. 2A).

Supporting a direct effect of fatty acids on hepatic CEACAM1 expression, treating primary hepatocytes with 0.1 mM of a fatty acid mixture (FA) with a composition resembling that of the dietary fat reduced CEACAM1 protein level (Fig. 2C-ii). Consistent with our previous observations (12), the downregulatory effect of FA appears to be mediated by Pparα activation, as demonstrated by the ability of FA (0.1 mM) to reduce the transcriptional activity of Ceacam1 WT promoter (−1,100), but not of the construct harboring a mutation of the sole active Ppar response element (PPRE/RXR) located between nucleotides –557 and –543 (Fig. 2D).

NA restores lipid metabolism in the liver of mice fed an HF diet

HF increased fat accumulation in liver, as shown by H and E analysis (**Fig. 3A**, HF-S vs. RD-S) and the high hepatic triacylglycerol content (Table 1). While this could be attributed, at least in part, to reduced fatty acid flux from the adipose tissue to the liver, we investigated whether NA could also affect fatty acid synthesis and β-oxidation in liver. Given the ∼3-fold increase in hepatic fatty acid oxidation in HF-S (Fig. 3B; 3.31 ± 0.22 vs. 1.07 ± 0.07 nmol/g/min in RD-S; $P < 0.05$), hepatic steatosis could in part, result from elevated Fasn protein levels (Fig. 3C-ii), and activity (Fig. 3C-i) in response to basal hyperinsulinemia (Fig. 2B-i) (37). NA treatment significantly reversed fat accumulation in liver (Fig. 3A; HF-NA vs. HF-S) and hepatic triacylglycerol levels (Table 1; HF-NA vs. HF-S) in parallel to reversing basal hyperinsulinemia (Fig. 2B-i) and Fasn level (Fig. 3C-ii). Consistent with a previous report (11), the acute rise of insulin release at refeeding (RF) downregulates Fasn activity relative to fasting (F) in RD-S mice (Fig. 3C-i). This occurred in parallel to induced CEACAM1 phosphorylation as shown by immunoblotting with anti-phospho-CEACAM1 (α-pCC1) antibody (Fig. 3C-ii), followed by its increased binding to Fasn, as shown by its detection in coimmunoprecipitation (Co-IP) with the Fasn immunopellet from RD-S mice (Fig. 3C-iii). In contrast, under chronic hyperinsulinemic conditions and in response to HF, insulin failed to phosphorylate CEACAM1 and induce its binding to Fasn to decrease its activity in HF-S. In HF-fed mice, NA restored refeeding-induced CEACAM1 phosphorylation (Fig. 3C-ii) and its binding to Fasn (Fig. 3C-iii) to downregulate its activity (Fig. 3C-i). Together with maintaining the rise in fatty acid β-oxidation (Fig. 3B; 4.39 ± 0.52 in HF-NA vs. 1.07 ± 0.07 nmol/g/min in RD-S; $P < 0.05$), NA's ability to restore the suppressive effect of insulin on Fasn activity could counter the effect of HF diet on fat deposition in liver.

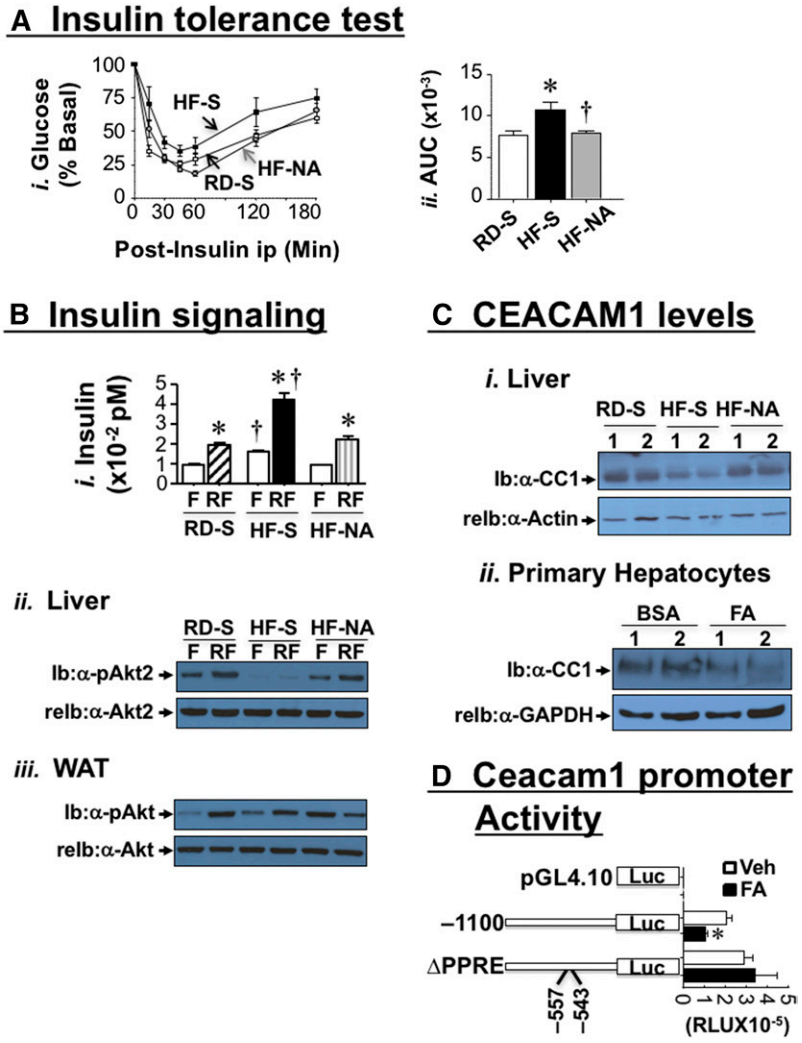

Fig. 2. Effect of NA on metabolism and insulin signaling. A-*i:* RD-fed mice were injected with saline (RD-S, white square) and HF-fed mice with saline (HF-S, black square) or NA (HF-NA, gray circle) before intraperitoneal insulin tolerance test was carried out to measure glucose disposal at 0–180 min. *ii:* The AUC was calculated. n = 6–10 mice/feeding/treatment group. Values are expressed as mean ± SEM. * $P < 0.05$ versus RD-S (white bar); † $P < 0.05$ HF-NA (gray bar) versus HF-S (black bar). B: At the end of feeding/treatment period, mice were fasted overnight (F, white bar) and then refed (RF) for 7 h to measure plasma insulin level (*i*). Western analysis in liver (*ii*) and WAT lysates (*iii*) was carried out by immunoblotting (Ib) with α-phospho-Akt (α-pAkt) antibodies, followed by reimmunoblotting (re-Ib) with α-Akt antibody to normalize per total Akt loaded. Gels represent 2 independent experiments on 2 mice/feeding/treatment group. C-*i*: Liver lysates were analyzed by Western Blotting, probed with α-CEACAM1 (α-CC1), followed by α-Actin antibody. *ii:* Hepatocytes were isolated from WT mice and treated with either BSA or with BSA-coupled fatty acid mixture (FA) (0.1 mM), lysed, and analyzed by Western blot, using immunoblotting (Ib) with α-CC1, followed by α-GAPDH antibody for normalization. Gel represents three independent experiments. D: Constructs from the mouse promoter bearing the WT sequence from nt −1,100 to +30 or a block mutation of the only active PPRE/RXR site located between nt −557 and −543 were generated, subcloned into the pGL4.10 promoterless plasmid before their Luciferase activity in response to ethanol (Veh) (white bars) or FA (0.1 mM) (black bars) was determined in mouse Hepa1-6 cells. As a negative control, cells were transfected with the empty pGL4.10. The experiment was performed in quadruplet several times. Luciferase light units were expressed as mean ± SD in relative light units (RLU). The graph represents typical results from several separate experiments. * $P < 0.05$ versus Veh-treated cells (black vs. white bar per each construct).

Hepatic adenoviral-redelivery of CEACAM1 reverses diet-induced metabolic abnormalities

We then tested whether reduced hepatic CEACAM1 is critical to diet-induced metabolic abnormalities. To this end, we rescued CEACAM1 in the liver using adenoviral-mediated redelivery (Ad) and examined whether this reversed the abnormal diet-induced metabolic phenotype. Mice fed HF for 21 days were injected with comparable titers of Ad-GFP control, adenovirus construct bearing WT rat CEACAM1 cDNA (Ad-rWT), and the adenovirus construct bearing the S503A phosphorylation-defective CEACAM1 mutant cDNA (Ad-rSA). Immunoblotting tissue lysates 3 days postadenoviral injection with α-mouse CEACAM1 antibody detected endogenous CEACAM1

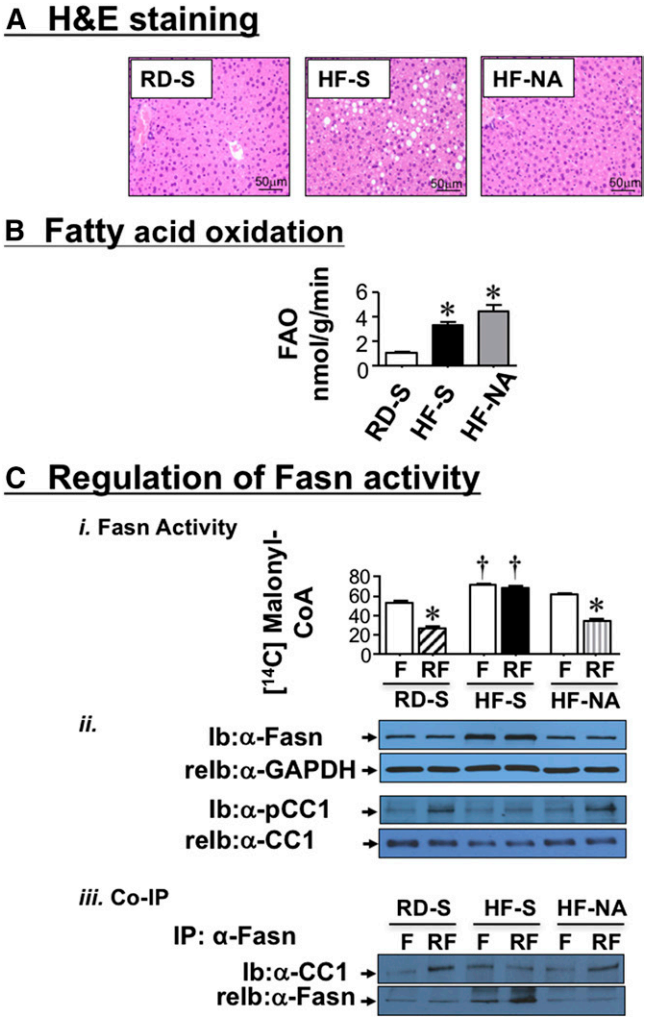

Fig. 3. Effect of NA on lipid metabolism in liver. A: Liver histology was assessed by H and E stained sections (n = 5 mice/feeding/treatment group). HF-S mice exhibit microvesicular lipid infiltration alternating with normal liver parenchyma. HF-NA manifested a normal histology like that of RD-S. Representative images from three sections/mouse are shown (20× magnification). B: Hepatic fatty acid oxidation was determined in 4 mice/feeding/treatment group. Experiments were repeated at least three times. Values are expressed as mean ± SEM. * $P < 0.05$ versus RD-S. C-*i*: Fasn enzymatic activity was measured in the liver by [^{14}C]malonyl-CoA incorporation on mice that had been fasted overnight (F) and refed for 7 h (RF). n = 5/feeding/treatment group. Each assay was performed in triplicate. Values are expressed as mean ± SEM. * $P < 0.05$ versus F/each treatment group; † $P < 0.05$ versus F or RF in other treatment groups. *ii*: Western analysis of Fasn (normalized to GAPDH) and phosphorylated CEACAM1 normalized to total CEACAM1 in liver lysates. *iii*: Co-IP analysis of Fasn binding to CEACAM1 was carried out by immunoprecipitating (IP) with α-Fasn antibody followed by immunoblotting (Ib) with α-CC1 antibody. Gels represent more than two separate experiments.

protein expression in liver, with insignificant expression in WAT and skeletal muscle (**Fig. 4A**-i, mCC1), as expected from the limited expression of CEACAM1 in these tissues (9). In contrast, immunoblotting with α-rat CEACAM1 antibody revealed restricted expression of rat CEACAM1 (rCC1) to the liver but not WAT or muscle of mice injected with Ad-rWT or Ad-rSA, but not Ad-GFP. Transgenic rat CEACAM1 expression was sustained for at least 21 days, as demonstrated by Western (Fig. 4A-ii) and qRT-PCR (Fig. 4A-iii) analyses of liver lysates. Per our earlier report (17), endogenous mouse Ceacam1 mRNA (Fig. 4A-iii) and CEACAM1 protein (Fig. 4A-ii) content were reduced by >60% by HF. In parallel, HF impaired insulin clearance, as assessed by steady-state C-peptide/insulin molar ratio, and hyperinsulinemia (**Table 2**, HF-GFP vs. RD-GFP). This caused fed hyperglycemia (Table 2), and intolerance to insulin (Fig. 4B-i, blue vs. black lanes and AUC bars) and glucose (Fig. 4B-ii), as assessed on day 13 and 16 postinjection, respectively. Ad-rWT delivery restored insulin clearance together with plasma insulin and C-peptide levels in HF-fed mice (Table 2, HF-rWT vs. RD-GFP). It also restored insulin and glucose tolerance (Fig. 4B-i and ii, respectively, green vs. black lanes and AUC bars) and blood glucose levels (Table 2). In contrast, injecting Ad-rSA CEACAM1 mutant (red) failed to restore these metabolic factors (Table 2 and Fig. 4B).

Consistent with the positive effect of hyperinsulinemia on hepatic de novo lipogenesis (37), HF-GFP mice manifested higher mRNA levels of sterol regulatory element-binding protein-1c, the master transcriptional regulator of lipogenic genes, than RD-GFP (supplemental Table S3). This increased Fasn mRNA (supplemental Table S3) and protein content (**Fig. 5A**-i) in the liver and subsequently, enzymatic activity (Fig. 5A-ii).

Additionally, HF induced mRNA levels of genes implicated in fatty acid transport, such as Fatp-1 and Fatp-4 (supplemental Table S3, HF-GFP vs. RD-GFP). In contrast, HF lowered carnitine palmitoyltransferase-1α (Cpt-1α) mRNA levels (supplemental Table S3). Consistent with the role of CPT-1α in transporting fatty acids to mitochondria for β-oxidation, hepatic mRNA expression (supplemental Table S3) and plasma levels of FGF21 (Table 2) were ∼2-fold lower in HF-GFP than RD-GFP mice. Injecting Ad-rWT, but not Ad-rSA, normalized the level of these genes (supplemental Table S3) as well as plasma FGF21 in HF-rWT, but not HF-rSA mice (Table 2), further supporting restored fatty acid β-oxidation by Ad-rWT redelivery. Together, this yielded limited fat accumulation in the liver of HF-rWT relative to HF-GFP and HF-rSA mice, as shown by histological analysis of the H and E stain of the liver (Fig. 5B), and by hepatic triacylglycerol content (Table 2). Consistent with redistribution of substrates to WAT, adipocytes' expansion was also restricted in HF-rWT by comparison to HF-GFP mice (Fig. 5C), as opposed to mice injected with Ad-rSA mutant in which adipocytes' expansion was comparable to that in Ad-GFP controls (Fig. 5C).

Consistent with enhanced inflammation by increased fat accumulation (38), qRT-PCR analysis showed induced pro-inflammatory (F4/80 and Tnf-α), and profibrotic genes (α-Sma and Col6α3) in the liver (supplemental Table S3) of HF-GFP versus RD-GFP mice, all of which were reversed by Ad-rWT, but not Ad-rSA injection. Of note, qRT-PCR analysis showed comparable mRNA levels of F4/80 and TNF-α in the liver of HF-fed mice 3 days postinjection of Ad-rWT and Ad-rSA CEACAM1 (supplemental Table S4). This indicates that the changes in the inflammatory signals

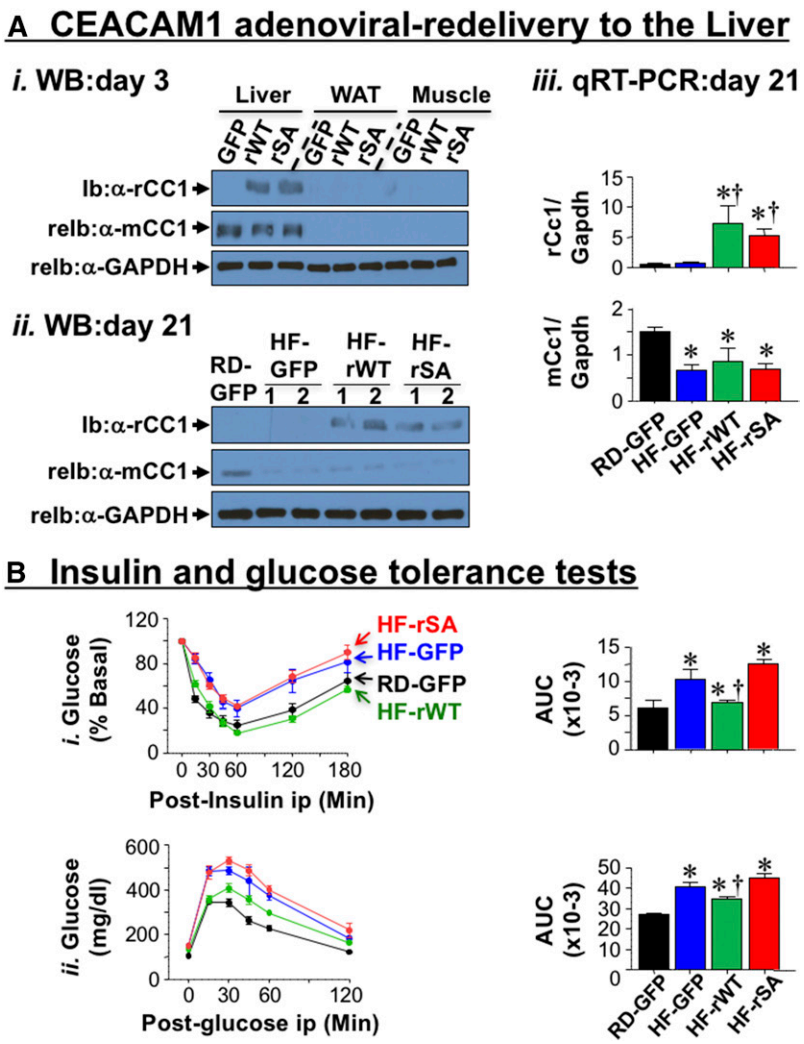

Fig. 4. Effect of adenoviral-mediated redelivery of CEACAM1 on glucose and insulin intolerance caused by HF diet. A-*i*: Western analysis of rat and mouse CEACAM1 expression (rCC1 and mCC1, respectively) in lysates from liver, WAT and skeletal muscle of 2-month-old RD-fed WT mice 3 days postinjection with Ad-GFP, Ad-rWT, and Ad-rSA. Membranes were reprobed with α-GAPDH antibody for normalization. *ii*: Western analysis (n = 2/each group) on liver lysates from mice fed with RD or HF for 41 days and injected with adenoviral particles in the last 21 days of feeding. *iii:* qRT-PCR analysis of liver lysates to measure rat and mouse Ceacam1 mRNA levels normalized to Gapdh (n = 5/each group in duplicate). B: Intraperitoneal insulin tolerance (*i*) and glucose tolerance (*ii*) tests were carried out 13 and 16 days, respectively, after being injected with Ad-GFP [black (RD) and blue (HF)], Ad-rWT (green), and Ad-rSA (red) (n = 6–8/per group). The AUC was measured and presented in graphs on the right. Values are expressed as means ± SEM. * $P < 0.05$ versus RD-fed; † $P < 0.05$ versus HF-GFP.

21 days postinjection are not related to the acute inflammatory response to adenoviral injection, but rather to the metabolic effect of WT CEACAM1, which appears to require longer than 3 days.

Consistent with the downregulation of Smad-7 expression by TNF-α (39), HF reduced the mRNA level of Smad-7 in WAT (supplemental Table S5, HF-GFP vs. RD-GFP). Redelivering Ad-rWT, but not Ad-rSA CEACAM1 to the liver restored Smad-7 levels (supplemental Table S5), consistent with possible TGF-β inhibition, as manifested by decrease in profibrotic genes, α-Sma and Col6α3, in the WAT of HF-rWT, but not HF-rSA mice (supplemental Table S5).

Adenoviral-redelivery of CEACAM1 rescues energy expenditure in HF-fed mice

Ad-rWT, but not Ad-rSA CEACAM1 totally reversed BW gain, visceral adiposity, and NEFA plasma levels (Table 2). It also restored the mRNA levels of UCP-1, a marker of brown adipogenesis, in WAT (supplemental Table S5). Additionally, it reduced, but not fully restored total fat mass (Table 2, HF-rWT vs. RD-GFP). This provided impetus to investigate potential changes in energy balance by indirect calorimetry 21 days postinjection. As expected (17), HF feeding reduced daily food intake in all mouse groups relative to RD-GFP mice (**Fig. 6A**). Indirect calorimetry analysis over a 24 h period revealed lower energy expenditure (Fig. 6B, heat generation), O_2 consumption (VO_2) (not shown), CO_2 production (VCO_2) (not shown), calculated RER (Fig. 6C), and spontaneous locomotor activity along the combined X, Y, Z axes (Fig. 6D) in HF-GFP relative to RD-GFP mice. Injecting mice with Ad-rWT, but not Ad-rSA CEACAM1, reversed the negative effect of HF on energy expenditure and the spontaneous locomotor activity. Preserved energy expenditure and physical activity could contribute to lower fat mass and BW in HF-rWT than HF-rGFP and HF-rSA mice (Table 2).

DISCUSSION

HF diet causes a progressive decline in hepatic CEACAM1 levels reaching ~60% after 3 weeks, at which point, it impairs insulin clearance to cause hyperinsulinemia with attendant insulin resistance and hepatic steatosis (17). Conversely, protecting CEACAM1 by fat-inducible liver-specific CEACAM1 overexpression restricted the metabolic derangement caused by HF diet, including visceral obesity and disturbed energy balance (17). While these studies

TABLE 2. Effect of adenoviral-mediated CEACAM1 redelivery to the liver on plasma and tissue biochemistry

	RD-GFP	HF-GFP	HF-rWT	HF-rSA
BW (g)	24.2 ± 0.3	27.6 ± 1.0[a]	25.2 ± 0.4[b]	27.9 ± 0.5[a,c]
% Fat mass (NMR)	3.5 ± 0.4	12.0 ± 1.2[a]	8.0 ± 0.7[a,b]	14.2 ± 0.9[a,c]
% Lean mass (NMR)	70.6 ± 0.7	65.0 ± 1.1	66.3 ± 0.5	59.8 ± 1.3
% Visceral fat (WAT/BW)	1.5 ± 0.1	2.6 ± 0.4[a]	2.1 ± 0.1	3.4 ± 0.3[a,c]
% BAT/BW	0.31 ± 0.02	0.25 ± 0.02	0.30 ± 0.03	0.23 ± 0.01
Hepatic triacylglycerol (μg/mg)	55.4 ± 8.2	104.2 ± 18.1[a]	54.3 ± 6.9[b]	98.5 ± 15.6[a,c]
Plasma NEFA (mEq/l)	0.4 ± 0.0	0.5 ± 0.0[a]	0.4 ± 0.0[b]	0.5 ± 0.0[a,c]
Plasma triacylglycerol (mg/dl)	48.5 ± 3.8	44.7 ± 3.5	51.4 ± 4.0	49.6 ± 3.0
Plasma insulin (pM)	26.8 ± 2.4	52.3 ± 8.5[a]	32.1 ± 3.5[b]	57.0 ± 8.6[a,c]
Plasma C-peptide (pM)	193.6 ± 8.6	307.8 ± 58.3[a]	199.1 ± 7.7[b]	2297.4 ± 32.5[a,c]
Steady-state C-peptide/insulin	8.6 ± 0.6	5.2 ± 0.3[a]	7.0 ± 0.8[b]	4.4 ± 0.3[a,c]
Fasting blood glucose (mg/dl)	70 ± 5	71 ± 6	73 ± 4	83 ± 7
Fed blood glucose (mg/dl)	112 ± 4	128 ± 4[a]	117 ± 2[b]	131 ± 5[a,c]
Plasma FGF21 (pM)	11.2 ± 2.2	5.3 ± 1.1[a]	16.2 ± 3.0[b]	6.0 ± 1.2[a,c]

Male mice (n = 6–10/feeding/treatment group) were fed RD or HF diet for 20 days before being injected through the tail vein with comparable amounts of adenoviral particles of Ad-GFP (as control), Ad-rWT, and Ad-rSA while they were maintained on RD or HF diet. At the end of the experiments (21 days postinjection), mice were euthanized, and tissues and blood removed to carry out the same analyses described in the legend to Table 1. Values are expressed as mean ± SEM.

[a] $P < 0.05$ versus RD-GFP.

[b] $P < 0.05$ versus HF-GFP.

[c] $P < 0.05$ HF-rSA versus HF-rWT.

underscored the importance of CEACAM1-dependent hepatic insulin clearance in promoting insulin sensitivity, they did not fully identify the primary factors that cause diet-induced CEACAM1 repression or the cause-effect relationship between impaired insulin clearance and insulin resistance in response to HF diet. The current studies showed that redistribution of WAT-derived fatty acids to the liver during lipolysis mediated the suppressive effect of HF diet on hepatic CEACAM1 expression, and that restoring CEACAM1 function by adenoviral redelivery completely reversed diet-induced metabolic abnormalities.

Blocking lipolysis with NA caused adipocytes' expansion to accommodate fat retention in WAT. This tissue remodeling was likely facilitated by a parallel decrease in fibrosis, a cellular event commonly found in the white adipose depot of insulin-resistant, obese rodents (32, 33) and humans (34). The anti-fibrotic effect of NA could be mediated by the ~2-fold rise in IFN-γ (40) that could counter the profibrogenic effect of Col6α3 (33) and IL-6 (40), and by the combined effect of the rise in WAT-derived TNF-α and plasma leptin levels (41).

While NA treatment caused fat accumulation, triggered more inflammation, and blunted insulin signaling in WAT of mice fed a HF diet for 30 days, it protected hepatic insulin signaling together with systemic insulin response. In parallel, it protected hepatic CEACAM1 levels against HF diet, demonstrating that lipolysis mediated the decline in hepatic CEACAM1 expression. This is consistent with findings of compromised insulin clearance and insulin signaling in parallel to reduced CEACAM1 protein content in rats receiving an intralipid-heparin infusion (24).

Lipolysis could occur shortly after initiating HF intake due to dysregulated hypothalamic control in the absence of insulin resistance in WAT (22). Released fatty acids could then suppress hepatic CEACAM1 content, as suggested by their downregulatory effect on Ceacam1 promoter activity and on its protein level in primary hepatocytes. Acute rise in fatty acids can also activate protein kinase Cδ-mediated pathways to impair insulin signaling in liver (24), which would in turn, suppress insulin-mediated Ceacam1 transcription (42). We have shown that repression of CEACAM1 does not translate into systemic insulin resistance until about 3 weeks of HF feeding (43) when hepatic CEACAM1 content is reduced by >60% (17). Complete reversal of these metabolic abnormalities by rescuing WT CEACAM1 in the liver of mice kept on a HF diet demonstrates that the decrease in hepatic CEACAM1 plays a causative role in sustaining systemic insulin resistance and hepatic steatosis in response to HF diet.

The physiological consequence of reduced CEACAM1 expression by HF diet appears to maintain hepatic fatty acids β-oxidation at times of excessive energy supply. We have reported that CEACAM1 downregulates Fasn activity to prevent steatosis in liver (11). We have also shown that PPARα reduces Ceacam1 transcription to regulate fatty acid β-oxidation during the fasting-refeeding transition (12) and in response to fenofibrate treatment (44). Because fatty acids are the endogenous ligands of PPARα (45), it is conceivable that adipose tissue-derived fatty acids reduce CEACAM1 levels by a PPARα-mediated mechanism as shown by failure of fatty acids to downregulate the transcriptional activity of a promoter construct bearing a mutation on the active PPRE/RXR site in Ceacam1 promoter, as they did to the WT promoter. As recently shown (12), suppressing CEACAM1 would provide a positive feedback mechanism on β-oxidation as it is expected to alleviate the negative effect of CEACAM1 on Fasn activity (11) and subsequently, reduce malonyl-CoA level to relieve its inhibitory effect on fatty acids translocation to the mitochondria to undergo β-oxidation. This presents a novel mechanistic underpinning for the regulation of lipid oxidation by plasma fatty acids (46).

Adenoviral-redelivery of WT CEACAM1 in the liver restored insulin clearance and, subsequently, insulin sensitivity and

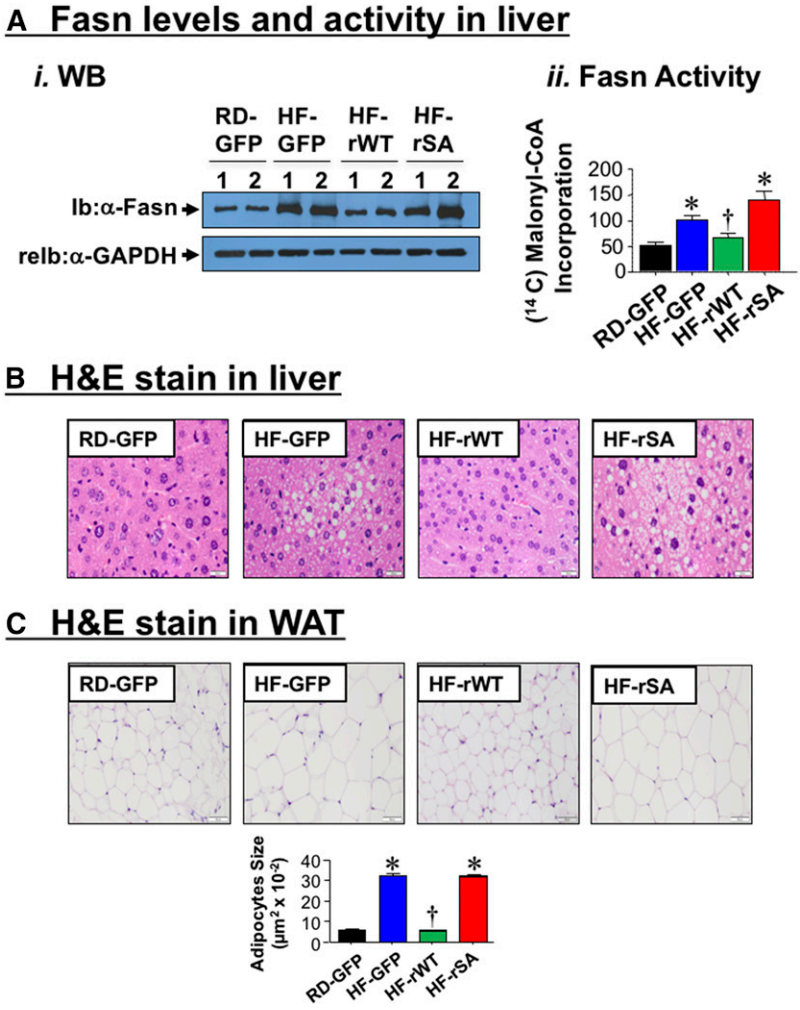

Fig. 5. Effect of adenoviral-mediated redelivery of CEACAM1 on diet-induced lipid alterations. A-*i*: Western analysis of Fasn levels in the liver lysates from mice fed with RD or HF for 41 days and injected with adenoviral particles in the last 21 days of feeding. *ii*: Fasn activity was assayed in liver lysates of RD-GFP (black), HF-GFP (blue), HF-rWT (green), or HF-rSA (red) (n = 6–8/per group). Values are expressed as mean ± SEM. * $P < 0.05$ versus RD-GFP; † $P < 0.05$ versus. HF-GFP. B: Liver histology was assessed by H and E stained sections (n = 5/each group). Whereas HF-GFP and HF-rSA exhibited microvesicular lipid infiltration alternating with normal liver parenchyma, RD-GFP and HF-rWT exhibited normal histology. Representative images from three sections/mouse are shown (40× magnification). C: H and E stain on WAT sections (n = 5/each group). HF diet caused enlarged adipocytes relative to RD-fed mice (HF-GFP vs. RD-GFP), as shown by the adipocyte size in the accompanying bar graph. This was reversed by Ad-rWT, but not Ad-rSA, injection. Representative images from three sections/mouse are shown (20× magnification), and values of adipocyte size are expressed as mean ± SEM. * $P < 0.05$ versus RD-GFP; † $P < 0.05$ versus HF-GFP.

normal lipid metabolism. It also restored locomotor activity and energy expenditure in mice fed a HF diet in parallel to reversing the gain in BW and visceral adiposity. Given that CEACAM1 is not produced by adipose tissue (9), it is likely that adenoviral delivery of CEACAM1 drives the expression of a set of factors that mediate this positive effect on energy expenditure and adipose tissue biology (reversal of adipocytes' expansion and limited fibrosis and inflammation). One of these factors might be the rise in plasma FGF21 (47, 48), which induces locomotor activity (49) to elevate energy dissipation (50, 51). Recapitulating the protective effect of forced expression of hepatic WT CEACAM1 on metabolism (17) and on adipose tissue biology and energy expenditure (30) in response to HF diet, the restorative metabolic effect caused by hepatic adenoviral redelivery of WT CEACAM1 on adipocytes supports the critical role of hepatocytic CEACAM1 in regulating insulin action and metabolism in other tissues.

Contrary to WT CEACAM1, adenoviral delivery of the Ad-rSA phosphorylation-defective CEACAM1 mutant failed to reverse the negative metabolic effects of HF diet. Using the L-SACC1 transgenic mouse with liver-specific dominant-negative overexpression of this SA phosphorylation-defective mutant, we demonstrated that impairment of insulin clearance causes chronic hyperinsulinemia followed by systemic insulin resistance and increased lipid production in liver and redistribution to adipose tissue to cause visceral obesity with increased lipolysis and FFA output (13). Consistent with downregulated insulin receptor by chronically elevated insulin levels (52, 53), L-SACC1 mice manifested reduced insulin receptor number and compromised insulin-induced signaling in hepatocytes (13) in addition to reduced ability of insulin to suppress hepatic glucose production, as demonstrated by hyperinsulinemic-euglycemic clamp analysis (54). Additionally, L-SACC1 mice developed insulin resistance including reduced glucose transport in muscle and adipose and increased lipid accumulation in liver and peripheral tissues (54). Hyperinsulinemia can cause insulin resistance in adipose tissue by reducing Glut4-mediated glucose transport (55). Moreover, chronic hyperinsulinemia can cause insulin resistance to the suppression of plasma FFA levels and increasing de novo lipogenesis but not with regard to hepatic gluconeogenesis (56). Hepatic insulin resistance and increased gluconeogenesis appear to be regulated by increased mobilization of FFA and adipokines from WAT (57, 58). Consistently, inhibiting lipolysis and inducing fatty acid oxidation restored insulin action in L-SACC1 transgenics (59), pointing to the role of altered fat metabolism in their sustained insulin resistance that was secondary

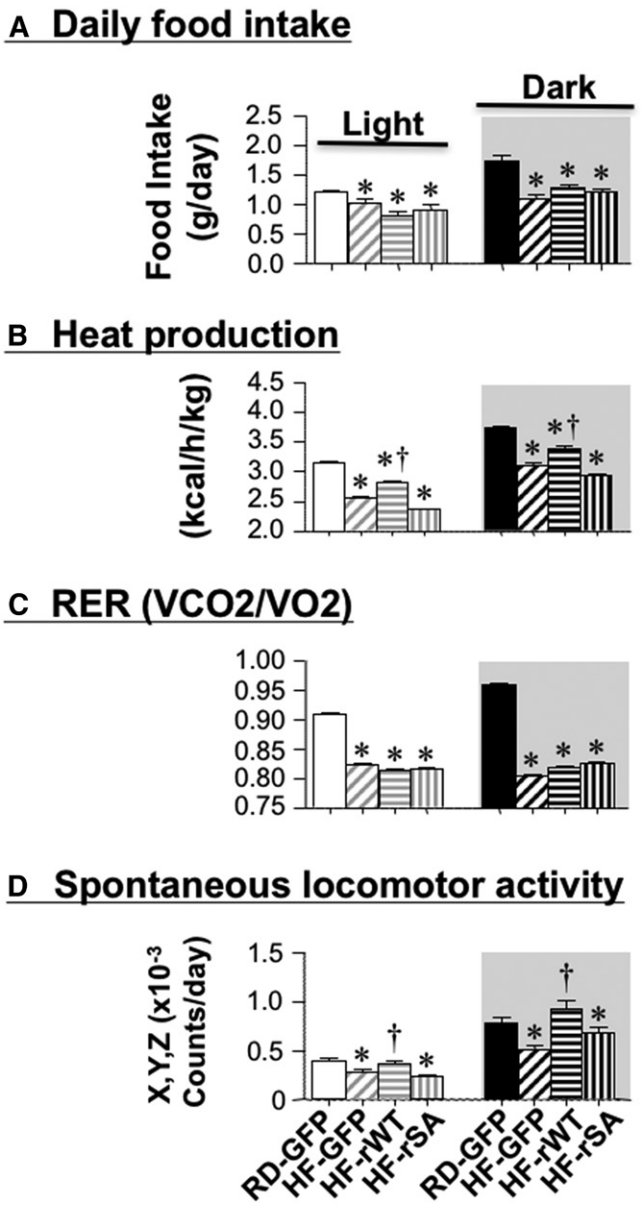

Fig. 6. Effect of adenoviral-mediated redelivery of CEACAM1 on diet-induced energy imbalance. Mice were individually caged (n = 4 per group), fed ad libitum, and subjected to indirect calorimetry analysis in a 24 h period for 5 days to measure: daily food intake (A); heat production (energy expenditure) (kcal/h/kg lean mass) (B); VCO_2 production and VO_2 consumption (mg/h/kg lean mass) to calculate RER as VCO_2/VO_2 ratio (C), and spontaneous locomotor activity along the X, Y, and Z axes (counts/day) (D). Values are expressed as mean ± SEM of each time interval in the last 3 days. * $P < 0.05$ versus RD-GFP per cycle; † $P < 0.05$ versus HF-GFP per cycle.

to impaired insulin clearance. Given that HF diet increases apoA1 (17), it is conceivable that elevated plasma FFA in L-SACC1 mice maintain the elevated level of the dominant-negative rat transgene expression driven by apoA1 promoter, while repressing that of the mouse endogenous gene by a PPARα-dependent mechanism (44). This could contribute to the suppression of endogenous CEACAM1 activity on hepatic insulin clearance and lipid metabolism by the S503A phosphorylation-defective Ceacam1 mutant transgene.

In summary, the current studies provide a novel role for hepatic CEACAM1-dependent pathways in regulating fatty acid metabolism along the adipocyte-hepatocyte axis in response to excess energy intake. Given that hepatic CEACAM1 content is markedly reduced in the liver of insulin-resistant obese subjects with fatty liver disease (20), the current findings propose that inducing CEACAM1 could constitute a critical therapeutic target that serves to mitigate diet-induced metabolic abnormalities, including obesity and fatty liver disease.

The authors thank Ms. M. Kopfman at the Najjar Laboratory for her technical assistance in the generation, genotyping, and maintenance of mice, in addition to carrying out routine RNA and DNA analyses.

REFERENCES

1. Dankner, R., A. Chetrit, M. H. Shanik, I. Raz, and J. Roth. 2009. Basal-state hyperinsulinemia in healthy normoglycemic adults is predictive of type 2 diabetes over a 24-year follow-up: a preliminary report. *Diabetes Care.* **32:** 1464–1466.
2. Pories, W. J., and G. L. Dohm. 2012. Diabetes: have we got it all wrong? Hyperinsulinism as the culprit: surgery provides the evidence. *Diabetes Care.* **35:** 2438–2442.
3. Corkey, B. E. 2012. Banting lecture 2011: hyperinsulinemia: cause or consequence? *Diabetes.* **61:** 4–13.
4. Ader, M., D. Stefanovski, S. P. Kim, J. M. Richey, V. Ionut, K. J. Catalano, K. Hucking, M. Ellmerer, G. Van Citters, I. R. Hsu, et al. 2014. Hepatic insulin clearance is the primary determinant of insulin sensitivity in the normal dog. *Obesity (Silver Spring).* **22:** 1238–1245.
5. Meistas, M. T., S. Margolis, and A. A. Kowarski. 1983. Hyperinsulinemia of obesity is due to decreased clearance of insulin. *Am. J. Physiol. Endocrinol. Metab.* **245:** E155–E159.
6. Jones, C. N., F. Abbasi, M. Carantoni, K. S. Polonsky, and G. M. Reaven. 2000. Roles of insulin resistance and obesity in regulation of plasma insulin concentrations. *Am. J. Physiol. Endocrinol. Metab.* **278:** E501–E508.
7. Pivovarova, O., W. Bernigau, T. Bobbert, F. Isken, M. Mohlig, J. Spranger, M. O. Weickert, M. Osterhoff, A. F. Pfeiffer, and N. Rudovich. 2013. Hepatic insulin clearance is closely related to metabolic syndrome components. *Diabetes Care.* **36:** 3779–3785.
8. Lee, C. C., S. M. Haffner, L. E. Wagenknecht, C. Lorenzo, J. M. Norris, R. N. Bergman, D. Stefanovski, A. M. Anderson, J. I. Rotter, M. O. Goodarzi, et al. 2013. Insulin clearance and the incidence of type 2 diabetes in Hispanics and African Americans: the IRAS Family Study. *Diabetes Care.* **36:** 901–907.
9. Najjar, S. M. 2002. Regulation of insulin action by CEACAM1. *Trends Endocrinol. Metab.* **13:** 240–245.
10. Choice, C. V., M. J. Howard, M. N. Poy, M. H. Hankin, and S. M. Najjar. 1998. Insulin stimulates pp120 endocytosis in cells co-expressing insulin receptors. *J. Biol. Chem.* **273:** 22194–22200.
11. Najjar, S. M., Y. Yang, M. A. Fernstrom, S. J. Lee, A. M. Deangelis, G. A. Rjaily, Q. Y. Al-Share, T. Dai, T. A. Miller, S. Ratnam, et al. 2005. Insulin acutely decreases hepatic fatty acid synthase activity. *Cell Metab.* **2:** 43–53.
12. Ramakrishnan, S. K., S. S. Khuder, Q. Y. Al-Share, L. Russo, S. L. Abdallah, P. R. Patel, G. Heinrich, H. T. Muturi, B. R. Mopidevi, A. M. Oyarce, et al. 2016. PPARalpha (peroxisome proliferator-activated receptor alpha) activation reduces hepatic CEACAM1 protein expression to regulate fatty acid oxidation during fasting-refeeding transition. *J. Biol. Chem.* **291:** 8121–8129.
13. Poy, M. N., Y. Yang, K. Rezaei, M. A. Fernstrom, A. D. Lee, Y. Kido, S. K. Erickson, and S. M. Najjar. 2002. CEACAM1 regulates insulin clearance in liver. *Nat. Genet.* **30:** 270–276.
14. Xu, E., M. J. Dubois, N. Leung, A. Charbonneau, C. Turbide, R. K. Avramoglu, L. DeMarte, M. Elchebly, T. Streichert, E. Levy, et al. 2009. Targeted disruption of carcinoembryonic antigen-related cell

adhesion molecule 1 promotes diet-induced hepatic steatosis and insulin resistance. *Endocrinology.* **150:** 3503–3512.
15. DeAngelis, A. M., G. Heinrich, T. Dai, T. A. Bowman, P. R. Patel, S. J. Lee, E. G. Hong, D. Y. Jung, A. Assmann, R. N. Kulkarni, et al. 2008. Carcinoembryonic antigen-related cell adhesion molecule 1: a link between insulin and lipid metabolism. *Diabetes.* **57:** 2296–2303.
16. Lee, S. J., G. Heinrich, L. Fedorova, Q. Y. Al-Share, K. J. Ledford, M. A. Fernstrom, M. F. McInerney, S. K. Erickson, C. Gatto-Weis, and S. M. Najjar. 2008. Development of nonalcoholic steatohepatitis in insulin-resistant liver-specific S503A carcinoembryonic antigen-related cell adhesion molecule 1 mutant mice. *Gastroenterology.* **135:** 2084–2095.
17. Al-Share, Q. Y., A. M. DeAngelis, S. G. Lester, T. A. Bowman, S. K. Ramakrishnan, S. L. Abdallah, L. Russo, P. R. Patel, M. K. Kaw, C. K. Raphael, et al. 2015. Forced hepatic overexpression of CEACAM1 curtails diet-induced insulin resistance. *Diabetes.* **64:** 2780–2790.
18. Mittelman, S. D., G. W. Van Citters, S. P. Kim, D. A. Davis, M. K. Dea, M. Hamilton-Wessler, and R. N. Bergman. 2000. Longitudinal compensation for fat-induced insulin resistance includes reduced insulin clearance and enhanced beta-cell response. *Diabetes.* **49:** 2116–2125.
19. Bakker, L. E. H., L. D. van Schinkel, B. Guigas, T. C. M. Streefland, J. T. Jonker, J. B. van Klinken, G. C. M. van der Zon, H. J. Lamb, J. W. A. Smit, H. Pijl, et al. 2014. A 5-day high-fat, high-calorie diet impairs insulin sensitivity in healthy, young South Asian men but not in Caucasian men. *Diabetes.* **63:** 248–258.
20. Lee, W. 2011. The CEACAM1 expression is decreased in the liver of severely obese patients with or without diabetes. *Diagn. Pathol.* **6:** 40.
21. Groop, L. C., C. Saloranta, M. Shank, R. C. Bonadonna, E. Ferrannini, and R. A. DeFronzo. 1991. The role of free fatty acid metabolism in the pathogenesis of insulin resistance in obesity and noninsulin-dependent diabetes mellitus. *J. Clin. Endocrinol. Metab.* **72:** 96–107.
22. Scherer, T., C. Lindtner, E. Zielinski, J. O'Hare, N. Filatova, and C. Buettner. 2012. Short term voluntary overfeeding disrupts brain insulin control of adipose tissue lipolysis. *J. Biol. Chem.* **287:** 33061–33069.
23. Kabir, M., K. J. Catalano, S. Ananthnarayan, S. P. Kim, G. W. Van Citters, M. K. Dea, and R. N. Bergman. 2005. Molecular evidence supporting the portal theory: a causative link between visceral adiposity and hepatic insulin resistance. *Am. J. Physiol. Endocrinol. Metab.* **288:** E454–E461.
24. Pereira, S., E. Park, Y. Mori, C. A. Haber, P. Han, T. Uchida, L. Stavar, A. I. Oprescu, K. Koulajian, A. Ivovic, et al. 2014. FFA-induced hepatic insulin resistance in vivo is mediated by PKCdelta, NADPH oxidase, and oxidative stress. *Am. J. Physiol. Endocrinol. Metab.* **307:** E34–E46.
25. Lee, Y. S., P. Li, J. Y. Huh, I. J. Hwang, M. Lu, J. I. Kim, M. Ham, S. Talukdar, A. Chen, W. J. Lu, et al. 2011. Inflammation is necessary for long-term but not short-term high-fat diet-induced insulin resistance. *Diabetes.* **60:** 2474–2483.
26. Girousse, A., G. Tavernier, C. Valle, C. Moro, N. Mejhert, A. L. Dinel, M. Houssier, B. Roussel, A. Besse-Patin, M. Combes, et al. 2013. Partial inhibition of adipose tissue lipolysis improves glucose metabolism and insulin sensitivity without alteration of fat mass. *PLoS Biol.* **11:** e1001485.
27. Wanders, D., E. C. Graff, B. D. White, and R. L. Judd. 2013. Niacin increases adiponectin and decreases adipose tissue inflammation in high fat diet-fed mice. *PLoS One.* **8:** e71285.
28. Heinrich, G., S. Ghosh, A. M. Deangelis, J. M. Schroeder-Gloeckler, P. R. Patel, T. R. Castaneda, S. Jeffers, A. D. Lee, D. Y. Jung, Z. Zhang, et al. 2010. Carcinoembryonic antigen-related cell adhesion molecule 2 controls energy balance and peripheral insulin action in mice. *Gastroenterology.* **139:** 644–652.
29. Hirschey, M. D., T. Shimazu, E. Goetzman, E. Jing, B. Schwer, D. B. Lombard, C. A. Grueter, C. Harris, S. Biddinger, O. R. Ilkayeva, et al. 2010. SIRT3 regulates mitochondrial fatty-acid oxidation by reversible enzyme deacetylation. *Nature.* **464:** 121–125.
30. Lester, S. G., L. Russo, S. S. Ghanem, S. S. Khuder, A. M. DeAngelis, E. L. Esakov, T. A. Bowman, G. Heinrich, Q. Y. Al-Share, M. F. McInerney, et al. 2015. Hepatic CEACAM1 over-expression protects against diet-induced fibrosis and inflammation in white adipose tissue. *Front. Endocrinol. (Lausanne).* **6:** 116–122.
31. Tong, X., K. Buelow, A. Guha, R. Rausch, and L. Yin. 2012. USP2a protein deubiquitinates and stabilizes the circadian protein CRY1 in response to inflammatory signals. *J. Biol. Chem.* **287:** 25280–25291.
32. Yadav, H., C. Quijano, A. K. Kamaraju, O. Gavrilova, R. Malek, W. Chen, P. Zerfas, D. Zhigang, E. C. Wright, C. Stuelten, et al. 2011. Protection from obesity and diabetes by blockade of TGF-beta/Smad3 signaling. *Cell Metab.* **14:** 67–79.
33. Sun, K., J. Park, O. T. Gupta, W. L. Holland, P. Auerbach, N. Zhang, R. Goncalves Marangoni, S. M. Nicoloro, M. P. Czech, J. Varga, et al. 2014. Endotrophin triggers adipose tissue fibrosis and metabolic dysfunction. *Nat. Commun.* **5:** 3485–3496.
34. Divoux, A., J. Tordjman, D. Lacasa, N. Veyrie, D. Hugol, A. Aissat, A. Basdevant, M. Guerre-Millo, C. Poitou, J. D. Zucker, et al. 2010. Fibrosis in human adipose tissue: composition, distribution, and link with lipid metabolism and fat mass loss. *Diabetes.* **59:** 2817–2825.
35. Nakao, A., M. Afrakhte, A. Moren, T. Nakayama, J. L. Christian, R. Heuchel, S. Itoh, M. Kawabata, N. E. Heldin, C. H. Heldin, et al. 1997. Identification of Smad7, a TGFbeta-inducible antagonist of TGF-beta signalling. *Nature.* **389:** 631–635.
36. Bitzer, M., G. von Gersdorff, D. Liang, A. Dominguez-Rosales, A. A. Beg, M. Rojkind, and E. P. Bottinger. 2000. A mechanism of suppression of TGF-beta/SMAD signaling by NF-kappa B/RelA. *Genes Dev.* **14:** 187–197.
37. Osborne, T. F. 2000. Sterol regulatory element-binding proteins (SREBPs): key regulators of nutritional homeostasis and insulin action. *J. Biol. Chem.* **275:** 32379–32382.
38. Najjar, S. M., and L. Russo. 2014. CEACAM1 loss links inflammation to insulin resistance in obesity and non-alcoholic steatohepatitis (NASH). *Semin. Immunopathol.* **36:** 55–71.
39. Nagarajan, R. P., F. Chen, W. Li, E. Vig, M. A. Harrington, H. Nakshatri, and Y. Chen. 2000. Repression of transforming-growth-factor-beta-mediated transcription by nuclear factor kappaB. *Biochem. J.* **348:** 591–596.
40. Bhogal, R. K., and C. A. Bona. 2005. B cells: no longer bystanders in liver fibrosis. *J. Clin. Invest.* **115:** 2962–2965.
41. Carter-Kent, C., N. N. Zein, and A. E. Feldstein. 2008. Cytokines in the pathogenesis of fatty liver and disease progression to steatohepatitis: implications for treatment. *Am. J. Gastroenterol.* **103:** 1036–1042.
42. Najjar, S. M., Y. Boisclair, Z. Nabih, N. Philippe, Y. Imai, Y. Suzuki, D. Suh, and G. Ooi. 1996. Cloning and characterization of a functional promoter of the rat pp120 gene, encoding a substrate of the insulin receptor tyrosine kinase. *J. Biol. Chem.* **271:** 8809–8817.
43. Park, S. Y., Y. R. Cho, H. J. Kim, T. Higashimori, C. Danton, M. K. Lee, A. Dey, B. Rothermel, Y. B. Kim, A. Kalinowski, et al. 2005. Unraveling the temporal pattern of diet-induced insulin resistance in individual organs and cardiac dysfunction in C57BL/6 mice. *Diabetes.* **54:** 3530–3540.
44. Ramakrishnan, S. K., L. Russo, S. S. Ghanem, P. R. Patel, A. M. Oyarce, G. Heinrich, and S. M. Najjar. 2016. Fenofibrate decreases insulin clearance and insulin secretion to maintain insulin sensitivity. *J. Biol. Chem.* In press.
45. Bays, H., L. Mandarino, and R. A. DeFronzo. 2004. Role of the adipocyte, free fatty acids, and ectopic fat in pathogenesis of type 2 diabetes mellitus: peroxisomal proliferator-activated receptor agonists provide a rational therapeutic approach. *J. Clin. Endocrinol. Metab.* **89:** 463–478.
46. Groop, L. C., R. C. Bonadonna, M. Shank, A. S. Petrides, and R. A. DeFronzo. 1991. Role of free fatty acids and insulin in determining free fatty acid and lipid oxidation in man. *J. Clin. Invest.* **87:** 83–89.
47. Emanuelli, B., S. G. Vienberg, G. Smyth, C. Cheng, K. I. Stanford, M. Arumugam, M. D. Michael, A. C. Adams, A. Kharitonenkov, and C. R. Kahn. 2014. Interplay between FGF21 and insulin action in the liver regulates metabolism. *J. Clin. Invest.* **124:** 515–527.
48. Owen, B. M., X. Ding, D. A. Morgan, K. C. Coate, A. L. Bookout, K. Rahmouni, S. A. Kliewer, and D. J. Mangelsdorf. 2014. FGF21 acts centrally to induce sympathetic nerve activity, energy expenditure, and weight loss. *Cell Metab.* **20:** 670–677.
49. Cornu, M., W. Oppliger, V. Albert, A. M. Robitaille, F. Trapani, L. Quagliata, T. Fuhrer, U. Sauer, L. Terracciano, and M. N. Hall. 2014. Hepatic mTORC1 controls locomotor activity, body temperature, and lipid metabolism through FGF21. *Proc. Natl. Acad. Sci. USA.* **111:** 11592–11599.
50. Rosenbaum, M., and R. L. Leibel. 1998. Leptin: a molecule integrating somatic energy stores, energy expenditure and fertility. *Trends Endocrinol. Metab.* **9:** 117–124.
51. Choi, M. S., Y. J. Kim, E. Y. Kwon, J. Y. Ryoo, S. R. Kim, and U. J. Jung. 2015. High-fat diet decreases energy expenditure and expression of genes controlling lipid metabolism, mitochondrial function and skeletal system development in the adipose tissue, along with

increased expression of extracellular matrix remodelling- and inflammation-related genes. *Br. J. Nutr.* **113:** 867–877.
52. Cook, J. R., F. Langlet, Y. Kido, and D. Accili. 2015. Pathogenesis of selective insulin resistance in isolated hepatocytes. *J. Biol. Chem.* **290:** 13972–13980.
53. Shanik, M. H., Y. Xu, J. Skrha, R. Dankner, Y. Zick, and J. Roth. 2008. Insulin resistance and hyperinsulinemia: is hyperinsulinemia the cart or the horse? *Diabetes Care.* **31 (Suppl. 2):** S262–S268.
54. Park, S. Y., Y. R. Cho, H. J. Kim, E. G. Hong, T. Higashimori, S. J. Lee, I. J. Goldberg, G. I. Shulman, S. M. Najjar, and J. K. Kim. 2006. Mechanism of glucose intolerance in mice with dominant negative mutation of CEACAM1. *Am. J. Physiol. Endocrinol. Metab.* **291:** E517–E524.
55. Gonzalez, E., E. Flier, D. Molle, D. Accili, and T. E. McGraw. 2011. Hyperinsulinemia leads to uncoupled insulin regulation of the GLUT4 glucose transporter and the FoxO1 transcription factor. *Proc. Natl. Acad. Sci. USA.* **108:** 10162–10167.
56. Koopmans, S. J., R. S. Kushwaha, and R. A. DeFronzo. 1999. Chronic physiologic hyperinsulinemia impairs suppression of plasma free fatty acids and increases de novo lipogenesis but does not cause dyslipidemia in conscious normal rats. *Metabolism.* **48:** 330–337.
57. Perry, R. J., J. P. Camporez, R. Kursawe, P. M. Titchenell, D. Zhang, C. J. Perry, M. J. Jurczak, A. Abudukadier, M. S. Han, X. M. Zhang, et al. 2015. Hepatic acetyl CoA links adipose tissue inflammation to hepatic insulin resistance and type 2 diabetes. *Cell.* **160:** 745–758.
58. Titchenell, P. M., W. J. Quinn, M. Lu, Q. Chu, W. Lu, C. Li, H. Chen, B. R. Monks, J. Chen, J. D. Rabinowitz, et al. 2016. Direct hepatocyte insulin signaling is required for lipogenesis but is dispensable for the suppression of glucose production. *Cell Metab.* **23:** 1154–1166.
59. Dai, T., G. A. Abou-Rjaily, Q. Y. Al-Share, Y. Yang, M. A. Fernstrom, A. M. Deangelis, A. D. Lee, L. Sweetman, A. Amato, M. Pasquali, et al. 2004. Interaction between altered insulin and lipid metabolism in CEACAM1-inactive transgenic mice. *J. Biol. Chem.* **279:** 45155–45161.